



Modified SiO as a high performance anode for Li-ion batteries

Yoon Hwa^a, Cheol-Min Park^b, Hun-Joon Sohn^{a,*}

^a Department of Materials Science and Engineering, Seoul National University, Seoul 151-744, Republic of Korea

^b School of Advanced Materials and System Engineering, Kumoh National Institute of Technology, Gumi, Gyeongbuk 730-701, Republic of Korea

HIGHLIGHTS

- ▶ The m-SiO is prepared using heat treatment followed by mechanical milling.
- ▶ The m-SiO is composed of nano Si embedded in a Si-suboxide/amorphous SiO₂ matrix.
- ▶ Ex-situ XRD and HRTEM have been performed to investigate the reaction mechanism.
- ▶ The m₁₀-SiO electrode exhibited ~1000 mAh g⁻¹ over 50 cycles.

ARTICLE INFO

Article history:

Received 22 June 2012

Received in revised form

21 August 2012

Accepted 22 August 2012

Available online 1 September 2012

Keywords:

Lithium ion battery

Anode

Silicon monoxide

Disproportionation reaction

ABSTRACT

An anode material with improved electrochemical performances for Li-ion batteries is prepared using the disproportionation reaction of SiO followed by a high energy mechanical milling process. The modified SiO is composed of embedded Si nano-crystallites in a Si-oxide matrix. Si-oxide matrix could be divided into two parts by reactivity with Li-ion. The inactive Si-suboxide matrix would buffer the volume expansion of embedded Si nano-crystallites and active amorphous SiO₂ during the lithiation. This modified SiO electrode shows a large reversible capacity, close to 1000 mAh g⁻¹, and good cyclability, over 50 cycles.

© 2012 Elsevier B.V. All rights reserved.

1. Introduction

Many studies have been conducted recently to enhance electrochemical properties of Li-ion batteries (LIBs), which are used widely in various electronic devices. The applications of LIBs have expanded into large units such as electrical vehicles and storage units, which demand much higher electrochemical performances, such as high power or large reversible capacity. Presently, conventional LIBs employ a carbonaceous material for anode material. However, carbonaceous anodes, especially graphite anodes have a small reversible capacity (LiC₆: 372 mAh g⁻¹) and a poor rate capability [1–3], and are not suitable for the new large units applications. Instead, Si-based materials have been studied actively because of the potential for use as Li-ion-battery anode material. Si has a very large theoretical capacity (at room temperature: Li₁₅Si₄: ~3600 mAh g⁻¹) at room temperature and a low

operating voltage [4–9]. However, in general, there are some problems in Si-based systems, such as drastic capacity fading due to a large volume change during the cycling and poor electrical conductivity [7–9].

Among the Si-based systems, SiO is one of the most attractive because of its high capacity and unique microstructure [10–18]. Solid SiO is thermodynamically unstable at all temperatures, and various models, such as a random bonding (RB) model [19], a random mixture (RM) model [20] and a Si-suboxide matrix concept [21,22] have been suggested. Although these models are still controversial, the Si-suboxide concept suggests that the SiO consists of amorphous Si and amorphous SiO₂ clusters surrounded by the Si-suboxide matrix. Because of this unstable state of solid SiO, the SiO could be transformed into a Si and SiO₂ during heat treatment and is called a disproportionation reaction [12,23,24]. Disproportionated SiO (d-SiO) is constituted of nano-crystallite Si and an amorphous Si-oxide matrix. The microstructure of d-SiO heat treated at 1200 °C, in particular, looked like a frog-spawn structure, with the Si nano-crystallites embedded in the amorphous Si-oxide matrix [12]. d-SiO showed different electrochemical

* Corresponding author. Tel.: +82 2 880 7226; fax: +82 2 885 9671.

E-mail address: hjsohn@snu.ac.kr (H.-J. Sohn).

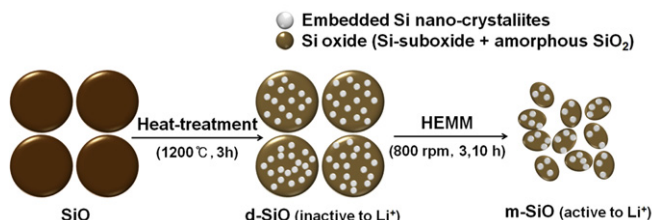


Fig. 1. Schematic illustration of the concept and preparation of m-SiO.

properties depending on the heat-treatment temperature [12]. It should be noted that the reaction mechanism of SiO is still controversial in many previous studies, such as those focused on the formation of a new phase (Li₂O, Li–Si alloys and Li–silicates), the reversibility of the phases, and the quantitative ratio of the final products [13–18].

In this work, SiO was disproportionated by heat treatment and modified using a high-energy mechanical milling (HEMM) process to enhance electrochemical properties for application as an anode material for LIBs. The HEMM method is a very simple process to reduce the particle size and to break the microstructure of material that may influence the electrochemical properties of other materials [25–27]. The active material–inactive matrix composite concept was applied to modify the d-SiO using HEMM method (m-SiO), which could improve the cyclability of electrodes since the

inactive matrix could act as a buffering matrix against the volume expansion/contraction during the cycling [28,29]. Also the reaction mechanism of m₁₀-SiO with Li was investigated.

2. Experimental

2.1. Synthesis

The d-SiO was prepared as follows. Commercial SiO (Aldrich, –325 mesh) was heat treated at 1200 °C for 12 h under an Ar atmosphere at a heating rate of 3 °C min^{–1}. After heat treatment, the furnace was cooled automatically to room temperature. For the preparation of m-SiO, the d-SiO was put into an 80 cm³ hardened steel vial with stainless steel balls (diameter: 3/8" and 3/16") at a ball-to-powder ratio of 20:1 and was milled at 800 rpm for 3 h or 10 h under Ar atmosphere using HEMM.

2.2. Electrochemical measurements

The test electrodes consisted of the active powder material (70 wt.%), carbon black (Ketchen Black, 15 wt.%) as a conducting agent and poly amide imide (PAI, 15 wt.%) dissolved in *N*-methyl pyrrolidinone (NMP) at 60 °C as a binder. Each component was well mixed to form slurry, using a magnetic stirrer. The slurry was coated on a copper foil substrate, pressed, and dried at 200 °C for 4 h under a vacuum. A coin-type electrochemical cell was used with Li foil as the counter and reference electrodes, and 1 M LiPF₆ and

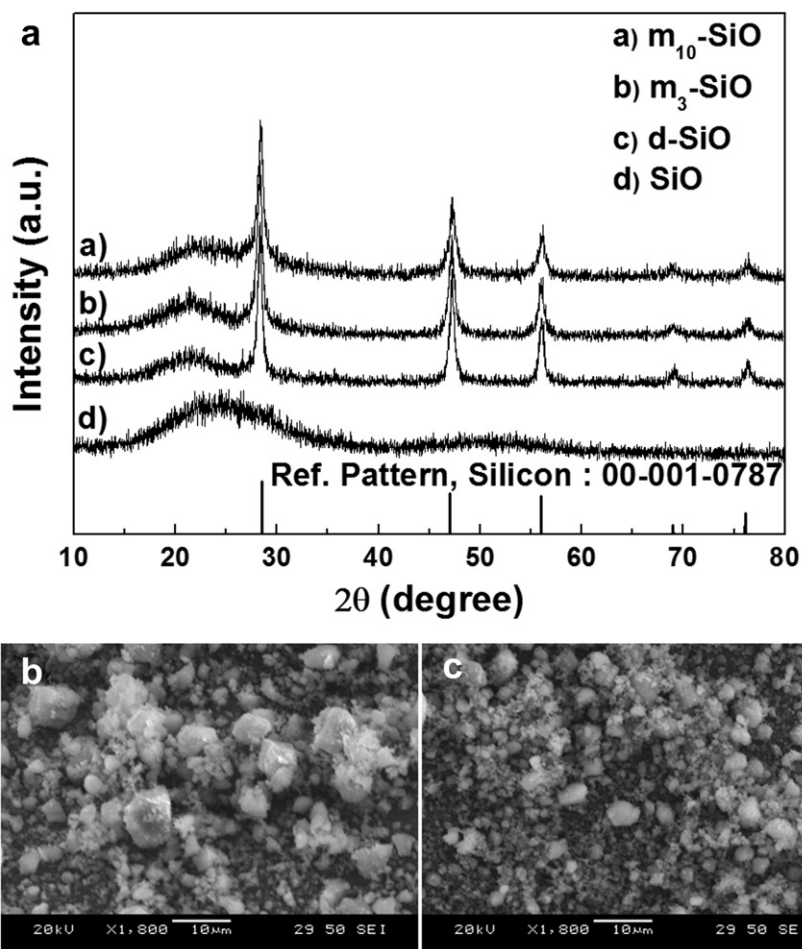


Fig. 2. (a) XRD patterns of SiO, d-SiO, and m-SiO. SEM images: (b) m₃-SiO and (c) m₁₀-SiO.

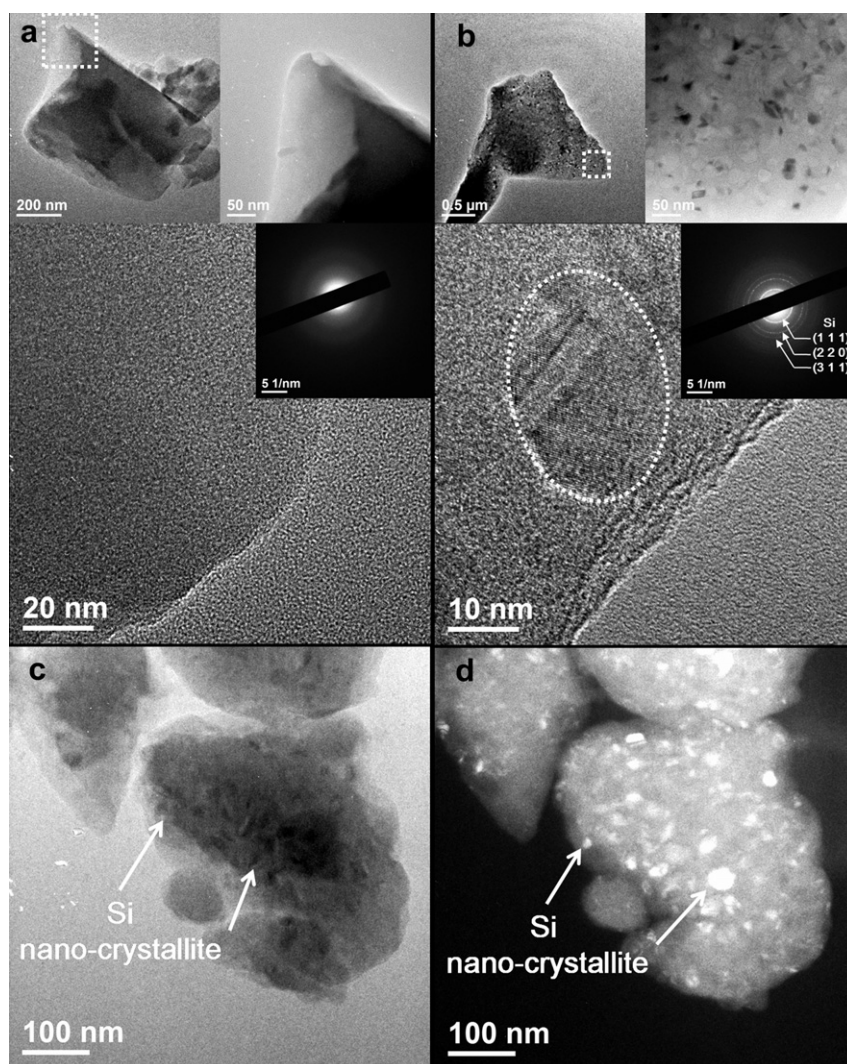


Fig. 3. Bright field, high-resolution TEM images, and SAED pattern: (a) SiO and (b) d-SiO. TEM images of m_{10} -SiO: (c) Bright field TEM image and (d) Dark field TEM image.

10% fluoro ethylene carbonate (FEC) in ethylene carbonate (EC)/diethyl carbonate (DEC) (3:7 (v/v), PANAX) as the electrolyte. The cell assembly and all of the electrochemical tests were carried out in an Ar-filled glove box.

The cycling experiments were galvanostatically performed using a Maccor automated tester at a constant current of 100 mA g^{-1} for the active material within the voltage range between 0.0 and 2.0 V (vs. Li/Li^+). During the discharging step, Li was inserted into the electrode while Li was extracted from the electrode during the charge.

2.3. Characterization

The SiO, d-SiO, and m-SiO samples were characterized using an X-ray diffractometer (XRD, Rigaku, D-MAX2500-PC) with $\text{Cu-K}\alpha$ radiation. X-ray photoelectron spectroscopy (XPS, Kratos, AXIS) analyses were conducted to identify the oxidation states of the SiO, d-SiO, and m_{10} -SiO. Ar gas sputtering was applied to etch the surface of the samples to a depth of 200 nm to avoid surface impurities in the samples. The deconvolution of the Si spectra was carried out by curve fitting the spectra using Gaussian–Lorentzian mixtures. Fourier transform infrared spectroscopy (FT-IR, Nicolet 6700) analyses were performed in attenuated total reflectance (ATR) mode. Also, the phases of the samples were identified with

a high-resolution transmission electron microscope (HRTEM, JEOL, JEM-3000F) operating at 300 kV. Ex-situ XRD and a transmission electron microscope (TEM) were used to observe the structural changes occurred in the active material during cycling. A scanning

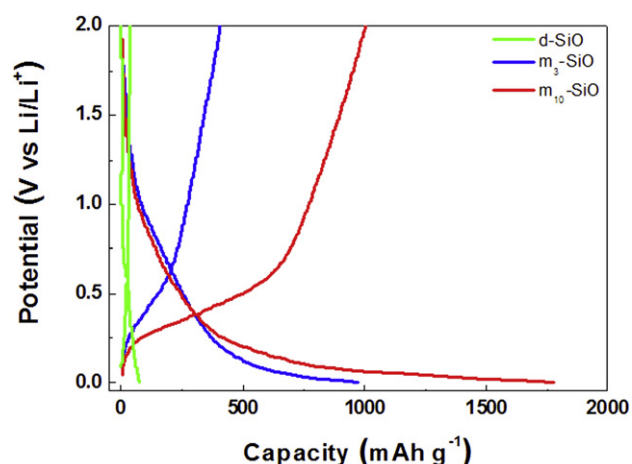


Fig. 4. Voltage profiles of d-SiO, m_3 -SiO, and m_{10} -SiO electrodes for the first cycle.

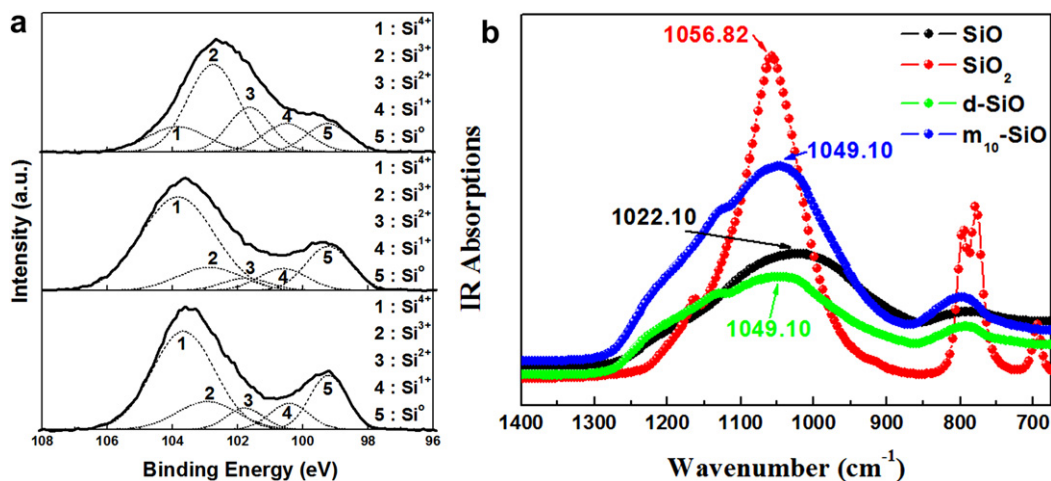


Fig. 5. (a) XPS spectra of SiO, d-SiO and m_{10} -SiO. (b) FT-IR spectra of SiO, SiO₂, d-SiO and m_{10} -SiO.

electron microscope (SEM, JSM-6360, JEOL) was employed to observe the particle size of the m -SiO. To prepare the ex-situ XRD samples, the electrodes were detached from the coin-type electrochemical cell, washed with diethyl carbonate (DEC), dried for 3 h in an Ar-filled glove box, and coated with Kapton tape, which served as a protective film. For ex-situ HRTEM analyses, samples were detached from the Cu substrate and were placed into a glass vial containing DEC solution. After ultrasonic treatment, a droplet of the DEC solution containing the dispersed active material particles was placed on a carbon-coated TEM grid. All XRD and HRTEM sample preparation processes were conducted in an Ar atmosphere glove box.

3. Results and discussion

Fig. 1 describes the sample preparation process for m -SiO. As mentioned previously, the basic concept is that the SiO would be disproportionated and Si nano-crystallites would be embedded in a Si-suboxide/amorphous SiO₂ composite matrix during the heat treatment. Since Si nano-crystallites and amorphous SiO₂ formed are surrounded with inactive Si-suboxide and did not react with Li in previous report [12], HEMM process is employed to break the Si-suboxide.

Fig. 2 shows XRD patterns and SEM images. In Fig. 2(a), when SiO is disproportionated at 1200 °C, sharp Si peaks appear in XRD patterns, and there are no changes in XRD patterns after the HEMM process for 3 h and 10 h (m_3 -SiO: milled for 3 h; m_{10} -SiO: milled for 10 h). SEM images of m_3 -SiO and m_{10} -SiO show the change of particle size due to the HEMM processing time in Fig. 2(b) and (c), respectively. The particle size of m_{10} -SiO is under 10 μ m, which is finer than that of the m_3 -SiO.

Fig. 3(a) and (b) shows HRTEM images and selected area electron diffraction (SAED) patterns of SiO and d-SiO, respectively. While the image and diffuse ring of the SAED pattern of SiO indicate an amorphous phase, embedded Si crystallites in an amorphous Si-

oxide matrix could be observed in the bright field image of d-SiO in Fig. 3(b). And the size of Si crystallites is about 20–30 nm. Bright and dark field TEM images of m_{10} -SiO are shown in Fig. 3(c) and (d), respectively. Due to the size reduction of particles during milling, embedded Si nano-crystallites are exposed at the surface of the

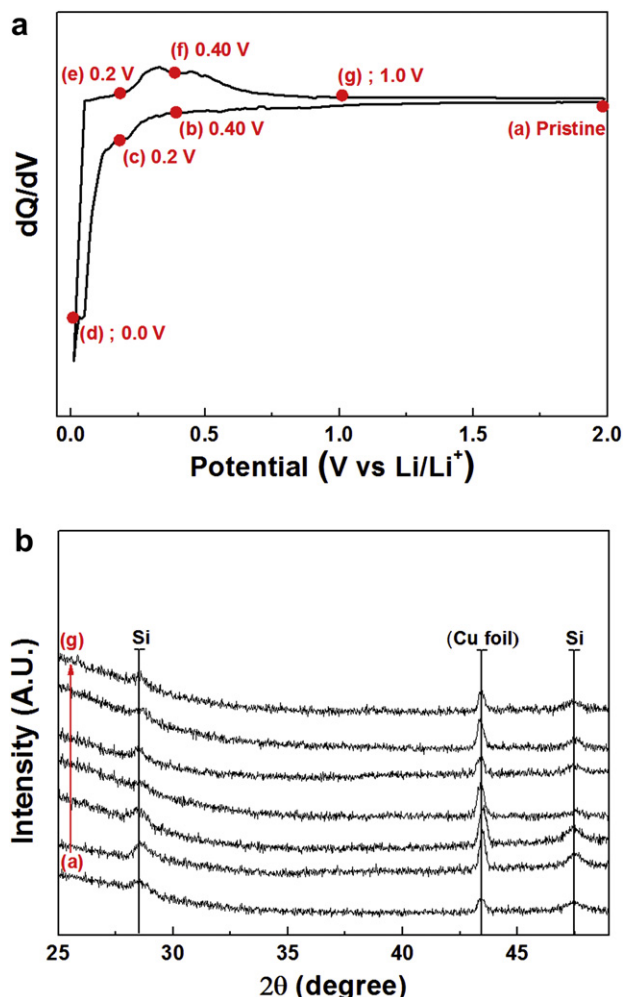


Fig. 6. (a) DCP and (b) XRD patterns of the m_{10} -SiO electrode at the first cycle.

Table 1
Abundance percentages for Si oxidation states of Si 2p spectra with SiO, d-SiO and m_{10} -SiO.

Sample	Si ⁰ (%)	Si ¹⁺ (%)	Si ²⁺ (%)	Si ³⁺ (%)	Si ⁴⁺ (%)
SiO	11.7	12.6	18.3	43.2	14.2
d-SiO	16.7	9.1	4.9	12.4	56.9
m_{10} -SiO	17.2	8.9	6.8	14.7	52.4

particle amenable to lithiation, from which the morphology of m-SiO is complied with the active material–inactive matrix composite concept shown in Fig. 1.

Electrochemical cell tests of m-SiO samples are carried out, and the results are shown in Fig. 4. The discharge and charge capacities of the m₃-SiO electrode are 969.2 mAh g⁻¹ and 406.5 mAh g⁻¹, respectively, while those of m₁₀-SiO are 1779 mAh g⁻¹ and 1001.8 mAh g⁻¹, respectively, at the first cycle. However, the d-SiO, heat-treated at 1200 °C is inactive to Li. The first cycle capacity of the d-SiO electrode only comes from carbon black, which is used as the conducting agent.

XPS analyses are conducted to identify the valence state of the Si 2p in SiO, d-SiO, and m₁₀-SiO, and the XPS results of the Si 2p spectra are shown in Fig. 5(a) and the amounts of Si oxidation states are summarized in Table 1. The results of XPS analyses agree with the previous work on d-SiO that the amount of Si⁰ (Si nanocrystallites) and Si⁴⁺ (amorphous SiO₂) states is increased after heat treatment [12]. The XPS spectrum and abundance percentages for Si oxidation states of Si 2p spectra with m₁₀-SiO are almost the same as those of d-SiO. FT-IR is employed in the absorbance mode, and the spectra are compared in Fig. 5(b). After the disproportionation reaction of SiO, peak is shifted close to the SiO₂ peak (1056.82 cm⁻¹) from the peak position of SiO (1022.10–1049.10 cm⁻¹). The peak position of m₁₀-SiO is the same with that of d-SiO (1049.10 cm⁻¹). According to the results of XPS (increase of Si⁴⁺ ratio) and FT-IR analyses (peak shift to the left), some parts of Si-suboxide in SiO particle changes to amorphous SiO₂ during heat treatment.

Fig. 6(a) is the differential capacity plot (DCP) of the m₁₀-SiO electrode when cycled between 2.0 and 0.0 V (vs. Li/Li⁺) for the first cycle. Ex-situ XRD and HRTEM analyses are performed to investigate the reaction mechanism of the m₁₀-SiO electrode at selected potentials as indicated in DCP. In Fig. 6(b), the XRD patterns show only Si peaks (28.5°, 47.5°) and Cu (foil) peaks, and there are no changes in the diffraction peaks during the first cycle except for a weakening of Si peak intensity at 0.0 V. And no peaks corresponding to Si–Li binary and Li–silicates phases are observed in XRD patterns.

Fig. 7(a)–(f) shows the HRTEM images with the fast Fourier transformed (FFT) patterns of the m₁₀-SiO electrode. When the potential is lowered to 0.4 V (Fig. 7(a)), only the Si crystallites could be identified. At 0.2 V (Fig. 7(b)), the Li₄SiO₄ phase is formed, which indicate the evidence of the existence of Li reacting amorphous Si-oxide. When the potential reached 0.0 V (Fig. 7(c)), the Li₂₁Si₈ phase and unreacted Si phase also appear. During the charge, the Li₂₁Si₈ phase disappears and the Si phase is observed at 0.2 V. When the potential is increased further, the Si and Li₄SiO₄ phases remained. According to previous studies on the reaction mechanism of SiO with Li, some Li-silicate phases are reported [13–17]. Among Li-silicates, the Li₄SiO₄ phase formed during the lithiation process is irreversible [18,30]. When the m₁₀-SiO electrode is electrochemically cycled, the Si phase is always observed even at the fully lithiated state (0.0 V), which agrees with the previous XRD analyses. This suggests that some of the Si nano-crystallites surrounded with Si-suboxide still exist after the HEMM process, and the Si nano-crystallites can't react with Li during the lithiation.

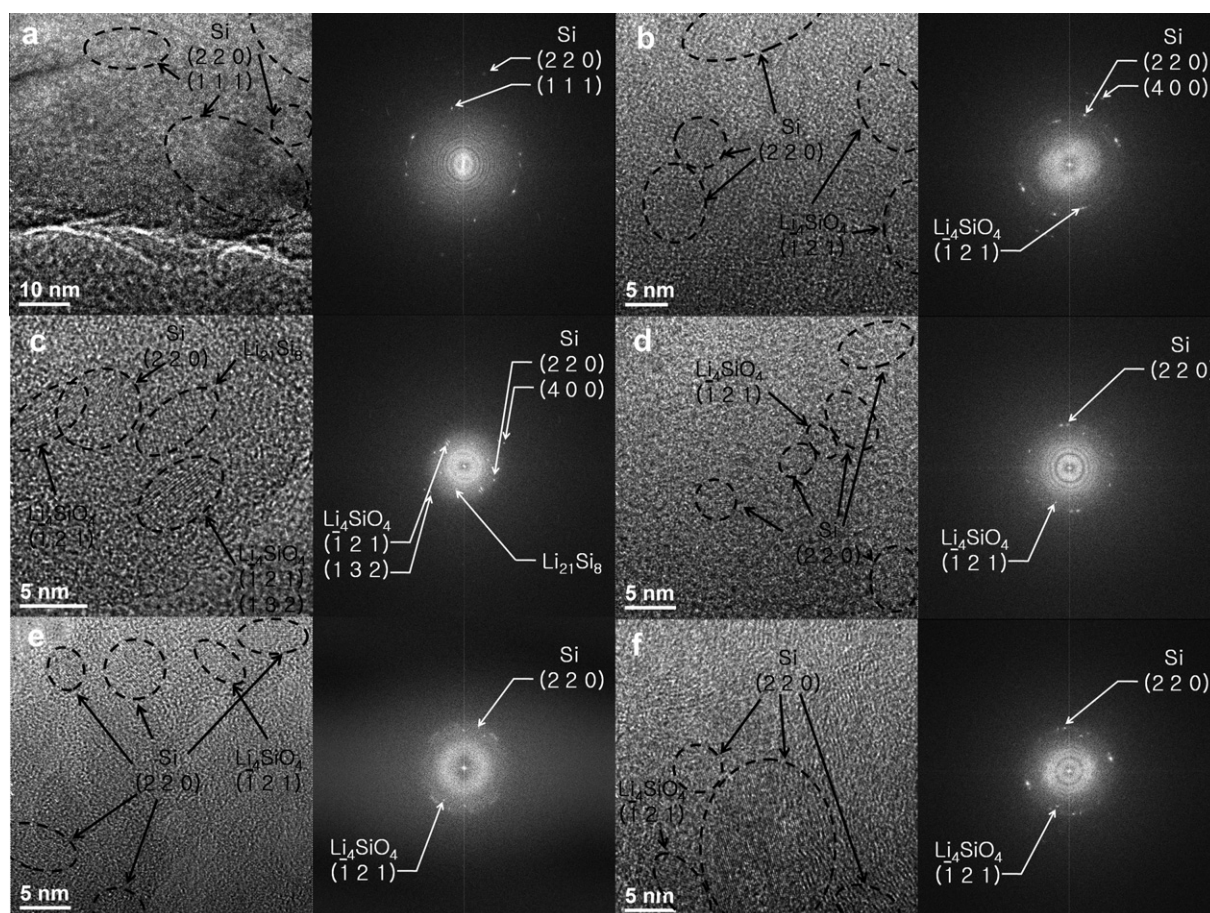


Fig. 7. Ex-situ HRTEM images with FFT patterns of the m₁₀-SiO electrode. Lithiation process: (a) 0.4 V, (b) 0.2 V, (c) 0 V, and the delithiation process: (d) 0.2 V; (e) 0.4 V; and (f) 1.0 V.

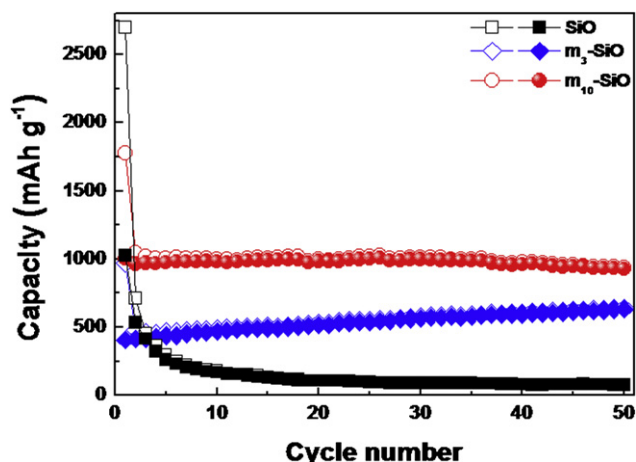


Fig. 8. The comparisons of the cyclabilities for the SiO, m_3 -SiO and m_{10} -SiO electrodes.

Based on the above results, Si-oxide matrix which surrounds the Si nano-crystallites could be divided into two parts by reactivity with Li ions as mentioned above. SiO which is disproportionated at 1200 °C doesn't react with Li in spite of the presence of embedded Si nano-crystallites since the Si suboxide surrounded the Si nano-crystallites and like a frog-spawn structure [12,15]. After the HEMM process, the Si-suboxide layer is partially broken, and the m-SiO can react with Li, and its reversible capacity increases with the HEMM processing time. Among Si-oxide matrix, an amorphous SiO_2 (Si^{4+}) phase can react with Li to form two Li silicate phases, Li_4SiO_4 and $\text{Li}_2\text{Si}_2\text{O}_5$ during the lithiation [30]. In this work, only Li_4SiO_4 phase is identified while $\text{Li}_2\text{Si}_2\text{O}_5$ phase is not detected. Other Si-suboxides might not react with Li.

Fig. 8 shows the comparison of cyclabilities of the SiO, m_3 -SiO, and m_{10} -SiO electrodes. The SiO electrode shows a very poor cyclability while m-SiO electrodes show better cyclability since SiO particle suffers a relatively large volume change during the cycling. However, volume change of m-SiO particles during the cycling is restrained by the Si-suboxide matrix, and the Si nano-crystallites and amorphous SiO_2 react with Li to form $\text{Li}_{21}\text{Si}_8$ and Li_4SiO_4 phases, respectively. In general, use of the carbon matrix in metal–carbon composites has shown better cycle retention and is easy to apply for various materials [31–33], but it affects charge capacity adversely [9]. Due to the excellent cyclability of the m-SiO electrode, it is not necessary to employ the carbon matrix for improvement of cycle retention in this case. Among the two m-SiO electrodes, the m_{10} -SiO electrode shows a much higher reversible capacity of $\sim 1000 \text{ mAh g}^{-1}$ during 50 cycles than that of the m_3 -SiO electrode ($\sim 500\text{--}600 \text{ mAh g}^{-1}$ during 50 cycles). The reversible capacity of the m_{10} -SiO is higher than that of the SiO/C composite reported [11,12]. This shows that the HEMM process is an effective method for decreasing the particle size of m-SiO, as shown in Fig. 2(c) and (d), and also for exposing the Si nano-crystallites and amorphous SiO_2 of the m_{10} -SiO to the electrolyte.

4. Conclusions

An m-SiO for use as a Li-ion battery anode material is prepared using the disproportionation reaction of SiO followed by the HEMM process. This m-SiO consists of embedded Si nano-crystallite and a Si-suboxide/amorphous SiO_2 composite matrix. During the lithiation step, Li_4SiO_4 and $\text{Li}_{21}\text{Si}_8$ phases appear while the Li_4SiO_4 phase is the irreversible. Among the samples tested, the m_{10} -SiO shows a high capacity of about 1000 mAh g^{-1} and good cycle retention without any carbon matrix. These results are attributed to the buffering effect of the Si-suboxide matrix against the volume change of the electrode during the cycling, and the m_{10} -SiO material could be a promising anode material for LIBs.

Acknowledgments

This work was supported by the research fund of the POSCO Chair Professor (H.-J. Sohn) at the Seoul National University.

References

- [1] J.R. Dahn, T. Zheng, Y. Liu, J.S. Xue, *Science* 270 (1995) 590.
- [2] M. Winter, J.O. Besenhard, M.E. Spahr, P. Novak, *Adv. Mater.* 10 (1998) 725.
- [3] X.Y. Song, K. Kinoshita, *J. Electrochem. Soc.* 145 (1996) L120.
- [4] C.J. Wen, R.A. Huggins, *J. Power Sources* 37 (1981) 271.
- [5] H. Jung, Y.-U. Kim, M.S. Sung, Y. Hwa, G. Jeong, G.B. Kim, H.-J. Sohn, *J. Mater. Chem.* 21 (2011) 11213.
- [6] A. Magasinski, P. Dixon, B. Hertzberg, A. Kvit, J. Ayala, G. Yushin, *Nat. Mater.* 9 (2010) 353.
- [7] M.N. Obrovac, L. Christensen, *Electrochem. Solid State Lett.* 7 (2004) A93.
- [8] J. Li, J.R. Dahn, *J. Electrochem. Soc.* 154 (2007) A156.
- [9] C.-M. Park, J.-H. Kim, H. Kim, H.-J. Sohn, *Chem. Soc. Rev.* 39 (2010) 3115.
- [10] J. Wang, K. Zhao, J. He, C. Wang, J. Wang, *J. Power Sources* 196 (2011) 4811.
- [11] J.-H. Kim, H.-J. Sohn, H. Kim, G. Jeong, W. Choi, *J. Power Sources* 170 (2007) 456.
- [12] C.-M. Park, W. Choi, Y. Hwa, J.-H. Kim, G. Jeong, H.-J. Sohn, *J. Mater. Chem.* 20 (2010) 4854.
- [13] M. Miyachi, H. Yamamoto, H. Kawai, T. Ohta, M.J. Shirakata, *J. Electrochem. Soc.* 152 (2005) A2089.
- [14] J. Yang, Y. Takeda, N. Imanishi, C. Capiglia, J.Y. Xie, O. Yamamoto, *Solid State Ionics* 152–153 (2002) 125.
- [15] M. Miyachi, H. Yamamoto, H. Kawai, *J. Electrochem. Soc.* 154 (2007) A376.
- [16] T. Kim, S. Park, S.M. Oh, *J. Electrochem. Soc.* 154 (2007) A1112.
- [17] Y. Nagao, H. Sakaguchi, H. Honda, T. Fukunaga, T. Esaka, *J. Electrochem. Soc.* 151 (2004) A1572.
- [18] J.-H. Kim, C.-M. Park, H. Kim, Y.-J. Kim, H.-J. Sohn, *J. Electroanal. Chem.* 1 (2011) 664.
- [19] H.R. Philipp, *J. Non-Cryst. Solids* 8–10 (1972) 627.
- [20] G.W. Brady, *J. Phys. Chem.* 63 (1959) 1119.
- [21] A. Hohl, T. Wieder, P.A. Aken, T.E. Weirich, G. Denninger, M. Vidal, S. Oswald, C. Deneke, J. Mayer, H. Fuess, *J. Non-Cryst. Solids* 320 (2003) 255.
- [22] K. Schulmeister, W. Mader, *J. Non-Cryst. Solids* 320 (2003) 143.
- [23] M. Mamiya, H. Takei, M. Kikuchi, C. Uyeda, *J. Cryst. Growth* 229 (2001) 457.
- [24] M. Mamiya, M. Kikuchi, H. Takei, *J. Cryst. Growth* 137 (2002) 1909.
- [25] C.-M. Park, S. Yoon, S.-I. Lee, H.-J. Sohn, *J. Power Sources* 186 (2009) 206.
- [26] J. Saint, M. Morcrette, D. Larcher, L. Laffont, S. Beattie, J.P. Peres, D. Talaga, M. Couzi, J.-M. Tarascon, *Adv. Funct. Mater.* 17 (2007) 1765.
- [27] C. Suryanarayana, *Prog. Mater. Sci.* 46 (2001) 1.
- [28] M.N. Obrovac, L. Christensen, D.B. Le, J.R. Dahn, *J. Electrochem. Soc.* 154 (2007) A849.
- [29] Y. Hwa, C.-M. Park, S. Yoon, H.-J. Sohn, *Electrochim. Acta* 55 (2010) 3324.
- [30] W.-S. Chang, C.-M. Park, J.-H. Kim, Y.-U. Kim, G. Jeong, H.-J. Sohn, *Energy Environ. Sci.* 5 (2012) 6895.
- [31] C.-M. Park, H.-J. Sohn, *Adv. Mater.* 19 (2007) 2465.
- [32] S.D. Beattie, D. Larcher, M. Morcrette, B. Simon, J.-M. Tarascon, *J. Electrochem. Soc.* 155 (2008) A158.
- [33] M. Yoshio, H.Y. Wang, K. Fukuda, T. Umeno, M. Dimov, Z. Ogumi, *J. Electrochem. Soc.* 149 (2002) A1598.